General Disclaimer

One or more of the Following Statements may affect this Document

- This document has been reproduced from the best copy furnished by the organizational source. It is being released in the interest of making available as much information as possible.

- This document may contain data, which exceeds the sheet parameters. It was furnished in this condition by the organizational source and is the best copy available.

- This document may contain tone-on-tone or color graphs, charts and/or pictures, which have been reproduced in black and white.

- This document is paginated as submitted by the original source.

- Portions of this document are not fully legible due to the historical nature of some of the material. However, it is the best reproduction available from the original submission.

On the Propagation and Interaction of Spherical Blast Waves

Max Kandula[1]
Sierra Lobo, Inc., Kennedy Space Center, FL 32899

Robert Freeman[2]
NASA Kennedy Space Center, FL 32899

The characteristics and the scaling laws of isolated spherical blast waves have been briefly reviewed. Both self-similar solutions and numerical solutions of isolated blast waves are discussed. Blast profiles in the near-field (strong shock region) and the far-field (weak shock region) are examined. Particular attention is directed at the blast overpressure and shock propagating speed. Consideration is also given to the interaction of spherical blast waves. Test data for the propagation and interaction of spherical blast waves emanating from explosives placed in the vicinity of a solid propellant stack are presented. These data are discussed with regard to the scaling laws concerning the decay of blast overpressure.

Nomenclature

c_0 = **ambient** sound speed, ft/s
d = distance from explosion, ft
e = internal energy per unit **mass**
E = total blast energy, lbf-ft
f = frequency, Hz
M = Mach number
M_s = shock Mach number
N = number of coalesced waves
p = static pressure, psia
p_0 = ambient pressure, psia
r = radial coordinate (distance from the source)
R = shock radius, ft
t = time, s
u = fluid or particle velocity, ft/s
U = shock velocity, ft/s
W_T = TNT equivalent weight of explosive, lb
Z = Brode's parameter, $d / W_T^{1/3}$ ($lb^{1/3}$)

Greek Symbols

α = 0,1,2 for plane, cylindrical, and spherical blast waves
γ = specific heat ratio
λ = $d/(E/p_0)^{1/3}$

[1] Sr. Principal Investigator, Mail Stop ASRC-5211, Associate Fellow AIAA.
[2] Launch Services Program, Associate Fellow AIAA.

ρ = density, lbm/ft^3
ξ = $r / R(t)$
η = $c_0^2 / \dot{R}^2 = 1 / M_s^2$
Δp = shock overpressure, psi

Subscripts

0 = upstream of shock (stationary)
1 = downstream of shock 9stationary)

C_p = pressure coefficient
Cx = force coefficient in the x direction
Cy = force coefficient in the y direction
c = chord
dt = time step
Fx = X component of the resultant pressure force acting on the vehicle
Fy = Y component of the resultant pressure force acting on the vehicle
f, g = generic functions
h = height
i = time index during navigation
j = waypoint index
K = trailing-edge (TE) nondimensional angular deflection rate

I. Introduction

The study of the propagation of blast waves in air is of great technical interest in many industrial applications- chemical, nuclear and aerospace. Blast waves are generated by point explosions (nuclear explosions and detonation of solid explosives, solid and liquid propellant rocket motors), high pressure gas containers (chemical explosions) and laser beam focusing in the ambient Blast wave problems also arise in astrophysics, hypersonic aerodynamics and hypervelocity impact. An understanding of the properties of the blast waves both in the near-field and the far-field is useful with regard to the characteristics such as blast overpressure, blast speed, and impulse.

Interesting problems also arise in the propagation and interaction (coalescence) of blast waves emanating from the detonation of closely spaced explosive charges (sequentially detonating, spatially distributed ammunition stacks). Regions of significant overpressure associated with the coalescence of blast waves from distributed ammunition stacks may be less extensive than regulatory requirements (Starkenberg and Benjamin[1]).

Many theoretical and experimental studies were reported by several investigators on the planar, cylindrical and spherical blast waves since the classical work of Taylor[2] on strong (intense) blast waves from nuclear explosions. The decay of blast wave amplitude (pressure, density or other physical properties behind the shock) has been studied less often (Diaci & Mozina[3,4]. This information will be useful in the possible detection of the source of the blast waves from far-field measurements. A proper understanding of the blast wave analysis and scaling is important in the interpretation of the test data.

This report summarizes the blast wave scaling laws and the characteristics of isolated spherical blast waves. Test data for the propagation and coalescence of blast waves from closely spaced multiple charges and solid propellant are examined and analyzed. Procedure for Paper Submission

II. Isolated Blast Wave Propagation

When disturbances of finite amplitude are propagated in perfect gases (destitute of viscosity or heat conductivity), discontinuities in pressure, velocity and temperature of the medium may occur. These are called shock waves (or shocks) or blast waves (intense shock waves). Shock waves and the flowfield become planar, cylindrically symmetric, or spherically symmetric, respectively if the energy source is in a plane, along a line, or at a point in space. The appearance of shocks is a consequence of nonlinear character of the equations governing the propagation

of finite disturbances that is in part responsible for the formation of discontinuities. This nonlinear character is evident from the temporal evolution of the pressure wave (**Fig.** 1).

Taylor[5,6], in his classical blast wave theory, formulated the equations of motion in Eulerian form for the spherical blast waves. He assumed instantaneous release of energy is released in an infinitely small region (**Fig.** 2a), that the ambient pressure is negligible compared to the shock overpressure (i.e. strong or intense shock wave), and that the variation of transport properties are unimportant. The resulting similarity solution is valid for very short times after the blast occurs.

Since the pioneering work of Taylor[6], several treatises and reviews have been published, notably those of Sakurai[7], Sedov[8], Openheim et al.[9], Kinney and Graham[10]. Sedov[11,8] and von Neumann[12] obtained an exact closed form analytical solution to the blast flowfield problem considered by Taylor (the sol-called Taylor problem). This solution is valid for very short times after the blast (the Taylor problem). At later times the strong shock assumption breaks down, and numerical methods are required for a solution (Director and Dabora[13]).

Sakurai[14,15] presented a perturbation solution to the general blast wave problem. An exact numerical solution of the blast wave problem covering strong and weak shock regions is provide by Goldstine and von Neumann[16]. Back and Lee[17] proposed an improved analytical solution to this problem.

Brode[18,19] numerically solved the Lagrangian equations in finite difference form with central differencing scheme. Both point sources and spheres of initially high pressure gas (**Fig.** 2b) and charges of TNT are considered.

A. Governing Equations

1. ***Eulerian Formulation***

The equations of motion (continuity, momentum and energy) for the flow of 1-D, inviscid, compressible gas in *Eulerian coordinates* are (Director and Dabora[13]):

$$\frac{\partial}{\partial t}\left(\rho r^{\alpha}\right)+\frac{\partial}{\partial r}\left(\rho r^{\alpha} u\right)=0 \tag{1a}$$

$$\frac{\partial}{\partial t}\left(\rho r^{\alpha} u\right)+\frac{\partial}{\partial r}\left\{\rho r^{\alpha}\left(u^{2}+\frac{p}{\rho}\right)\right\}=\alpha p r^{\alpha-1} \tag{1b}$$

$$\frac{\partial}{\partial t}\left\{\rho r^{\alpha}\left(e+\frac{u^{2}}{2}\right)\right\}+\frac{\partial}{\partial r}\left(\rho r^{\alpha} u\left\{e+\frac{u^{2}}{2}+\frac{p}{\rho}\right\}\right)=0 \tag{1c}$$

where r and t refer to space and time coordinates (independent variables), and e the internal energy per unit mass. The quantity α =0, 1, and 2 refers to planar, cylindrical, and spherical system respectively. The equation of state for a thermally perfect gas, supplementing the above equations, is expressed by

$$p=\rho e(\gamma-1) \tag{2}$$

where γ denotes the isentropic exponent, and is assumed constant.

2. *Lagrangian Formulation*

The mass contained within any region of space adjacent to the origin is

$$m=F_{0}\int_{0}^{r}\rho r^{\alpha}\,dr \tag{3}$$

where F_0=1, 2π, or 4π for plane, cylindrical or spherical system respectively. The conservation equations are transformed to Lagrangian form with the aid of the above equation as:

$$\frac{\partial}{\partial t}\left(\rho r^{\alpha}\right)+F_0\rho^2 r^{2\alpha}\frac{\partial u}{\partial m}=0 \tag{4a}$$

$$\frac{\partial u}{\partial t}+F_0 r^{\alpha}\frac{\partial p}{\partial m}=0 \tag{4b}$$

$$\frac{\partial\left(e+u^2/2\right)}{\partial t}+F_0\frac{\partial}{\partial m}\left\{r^{\alpha}up\right\}=0 \tag{4c}$$

3. *Rankine-Hugonoit Relations*

Behind the shock, a strong blast wind is initiated, which moves in the direction of the shock. The particle velocity acquired from the shock waves is obtained from the Rankine-Hugonoit relations. The Rankine-Hugonoit relations (boundary conditions) across a shock of finite strength at $r=R(t)$ are (Shapiro[20], p. 123; Liepmann & Roshko[21], p. 64), see **Fig.** 3 :

$$\frac{\rho_1}{\rho_0}=\frac{\gamma+1}{\gamma-1}\left\{\frac{2}{\gamma-1}\left(\frac{c_0}{U}\right)^2+1\right\}^{-1},\quad \frac{p_1}{p_0}=\frac{2\gamma}{\gamma+1}\left(\frac{U^2}{c_0^2}\right)-\frac{\gamma-1}{\gamma+1},\quad \frac{u_p}{U}=\frac{2}{\gamma+1}\left(1-\frac{c_0^2}{U^2}\right) \tag{5}$$

Here the shock velocity U (relative to the undisturbed gas; i.e. relative to a fixed coordinate system)

$$U=dR/dt \tag{6}$$

with R denoting the shock radius (or shock trajectory). The speed of sound in the undisturbed medium is defined as

$$c_0=\sqrt{\gamma p_0/\rho_0} \tag{7}$$

The shock Mach number M_s (=$U/c_0=u_0/c_0$) and the particle velocity u_p (near the shock) may be expressed in terms of the pressure ratio as

$$M_s^2=1+\left(\frac{p_1}{p_0}-1\right)\left(\frac{\gamma+1}{2\gamma}\right) \tag{8a}$$

$$\frac{u_p}{c_0}=\left(\frac{p_1}{p_0}-1\right)\left\{\frac{2\gamma/(\gamma+1)}{\frac{p_1}{p_{01}}+\frac{\gamma-1}{\gamma+1}}\right\}^{1/2} \tag{8b}$$

The quantity $P=\left(p_1/p_0-1\right)$ represents the strength of the shock, and $\Delta p=p_1-p_0$ denotes the overpressure.

Strong Shock Conditions

The strong shock conditions ($p_1>>p_0$, $U>>c_0$) simplify to

$$\frac{\rho_1}{\rho_0}=\frac{\gamma+1}{\gamma-1},\quad \frac{p_1}{p_0}=\frac{2\gamma}{\gamma+1}\frac{U^2}{a_0^2},\quad \frac{u_p}{U}=\frac{2}{\gamma+1} \tag{9}$$

In terms of the pressure ratio, the particle velocity may be expressed as

$$\frac{u_p}{c_0}=\sqrt{\frac{2}{\gamma(\gamma+1)}\frac{p_1}{p_{01}}} \tag{10}$$

B. Point Explosions

1. ***Strong Shock Solutions***

Self-similar solutions for the case of very strong shocks (short times after the explosion) were developed by Taylor[5,6] for spherical blast waves in his classical blast wave theory. These solutions are based on the form of the shock radius, which yield similarity solution. According to Taylor[2], a finite but large amount of energy is suddenly released by nuclear fission in an infinitely concentrated form. This leads to the formation of a shock wave according to

$$R(t)=S(\gamma)\rho_0^{-1/5}E^{1/5}t^{2/5}=S(\gamma)\left(t^2E/\rho_0\right)^{1/5} \tag{11}$$

which leads to a similarity solution. Here the quantity S is a dimensionless constant which is dependent on the specific heat ratio γ, and is determined by solving the equations of motion.

The governing partial differential equations (of continuity, momentum and energy) for a spherical wave (eqs. 1a-c in Eulerian form) are thereby reduced to an ordinary differential equation ODE, involving a single independent similarity variable defined by

$$\xi=r/R(t) \tag{12}$$

Rankine-Hugonoit relations for strong shock (eq. 9) are utilized. The total energy (kinetic energy and the heat energy) behind the shock is expressed by

$$E=4\pi\int_0^R\left(\frac{1}{2}\rho u^2\right)r^2\,dr+4\pi\int_0^R\frac{p}{\gamma-1}r^2\,dr \tag{13}$$

which is assumed *constant.* The constancy of energy in each $x-$sphere implies that the energy flowing into the sphere with the new material that enters it exactly balances the work which its original surface does by expanding it against the surrounding pressure. The boundary conditions include the condition that the particle velocity at the center of explosion must be zero.

Taylor[5,6] numerically solved the ODE. Taylor[2] solved the system for $\gamma=1.4$ numerically, starting from the condition at the shock $\eta=1$. An exact closed form analytical solution is given by Sedov[11], von Neumann[12], and later by J.L. Taylor[22]. Sedov[11] obtained solutions for plane, cylindrical and spherical blast waves, and for various values of γ. Von Neumann[12] sought a similarity solution for the point explosion (treated by Taylor) in Lagrangian formulation. The unknown shock boundary as a free surface is determined as part of the solution. The solution for the blast wave problem in Lagrangian coordinates is explicit in terms of the parameter $\theta=\varepsilon_c/\varepsilon_i$ (ratio of kinetic

and internal energies). This is in contrast to the implicit solution of the Eulerian equation of motion found by Sedov[11] and J.L. Taylor[12], see (**Sachdev** 2000).

Fig. 4a shows the prediction for the variation of the shock radius as a function of time, which is in close agreement with the measurements. The solutions (Sedov[11,8]) are shown in **Fig.** 4b, and exhibit three main features. The velocity curve ϕ rapidly becomes a straight line passing through the origin; 2. The density curve ψ approaches almost zero at $\eta \approx 0.5$, and remains close to it up to the center; 3. The pressure function f_1 decreases to become constant, and asymptotes to 0.37 times the maximum pressure just behind the shock. The very rapid decay of the density into the sphere is evident: almost all the gas is in a relatively thin layer behind the shock wave. This is due to the fact that the peak density of the gas immediately behind the shock ($\eta = 1$) has density **six** times the normal density, as given by the Rankine-Hugonoit relations (Landau & Lifshitz[23]). Most of the material in the blast wave gets accumulated near the shock. This tendency becomes more pronounced as $\gamma \to 1$.

An approximate analytical solution, which is explicit and instructive, was reported by Taylor[5] introduced a correction to the linear behavior of u by adding a nonlinear term. Taylor[5] integrated the ODE in a closed form for the case of spherical blast wave. The resulting solution is much closer to the numerical solution.

2. ***Shocks of Moderate Strength***

For intermediate times when the shock strength is finite, small departures from the classical solution due to counterpressure effects are accounted for in the perturbation solution by Sakurai[14], and in the quasi-similar solution of Oshima[24]. As the shock strength decreases with time, there is seen a negative pressure phase (expansion region) behind the shock (**Fig.** 5a). Exact numerical solutions (Sedov[8]) indicate an interesting feature, which is the development of a negative phase in the velocity distribution as the shock becomes weaker. Because the blast wave intensity decreases with time, the range ($x_t \le x \le x_f$) of the blast wave profile increases, and the magnitude of the pressure peaks (maximum and minimum) of the blast wave decreases (Chen & Liang[25]). **Fig.** 5b shows a typical pressure-time curve for the blast wave profile with a negative pressure region.

The shock radius in the limiting cases of strong shock limit ($p_2 > p_1$) and of acoustic limit corresponding to short and large distances are characterized by

$$R \propto t^{2/5} \quad \text{strong shock} \tag{14a}$$

$$R = c_0 t \quad \text{sound wave limit (at large distances)} \tag{14b}$$

a. Sakurai's solution[14,15,26]

Sakurai[14] generalized Taylor's similarity solution, and proposed a perturbation scheme for moderately strong shocks, in which the Taylor solution for strong shocks appears as the zeroth order solution. Sakurai expressed the solution in terms of two variables (also see Sedov[8], p. 297)

$$\xi = r / R(t), \quad \eta = [c_0 / U(t)]^2 = c_0^2 / \dot{R}^2 = 1/M_s^2 \tag{15}$$

The Rankine-Hugonoit equations for shocks of arbitrary strength (eq. 5) are utilized here. As in the strong shock case, the energy released E_α is assumed constant, and is expressed by

$$E_\alpha = \int_0^R \left\{ \frac{1}{2}u^2 + \frac{1}{\gamma - 1}\left(\frac{p}{\rho} - \frac{p_0}{\rho_0} \right) \right\} \rho r^\alpha \, dr, \qquad \alpha = 0,1,2 \tag{16}$$

where the $\alpha = 0$, 1 and 2 respectively corresponds to the plane, cylindrical and spherical blast waves. This represents the explosion energy per unit area of the surface of the shock when R equals unity. The Lagrangian form of the conservation of mass is

$$\int_0^R \frac{\rho}{\rho_0} r^\alpha \, dr = \frac{R^{\alpha+1}}{\alpha+1} \tag{17a}$$

Thus the equation for the total energy becomes

$$E_\alpha = \int_0^R \left(\frac{1}{2} u^2 + \frac{p}{\gamma - 1} \right) r^\alpha \, dr - \frac{p_0}{\gamma - 1} \frac{R^{\alpha+1}}{\alpha+1} \tag{17b}$$

The boundary conditions include the condition that the particle velocity at the center of explosion must be zero.

Numerical and approximate solutions are reported by Sakurai[14] for the zeroth and first order solution. The accuracy of the approximate solution for $\alpha = 0$ (plane) and 1 (cylindrical) for the zeroth order solution is remarkably good, the error being less than 5 percent (Sachdev[27], p. 65). With regard to the first order solution, the expansion of Sakurai[14] provided inaccurate results for $R \to \infty$ that are not consistent with the exact numerical solutions (Sachdev[27],p. 64).

Sakurai[26] developed an approximate solution in a manner similar to that of Taylor[5,6]. The assumptions of Sakurai[26] are that the particle velocity profile behind the shock is linear and that the derivative of the density with respect to the shock Mach number in the continuity equation is small and may be ignored. This assumption introduces serious error in the weak shock regime, where the shock wave gradually decays to become a sound wave (Sachdev[27], p. 64). The solution yields an asymptotic behavior for $R \to \infty$, which is at variance with the well-known results obtained in this limit by Whitham[28] and Landau[29]. It is not in good agreement with numerical solution, covering the entire range $0 < \phi < 1$. For the asymptotic motion at large times ($1/M_s^2 \to 1$). Solutions have been obtained by Whitham[28] and Sedov[8].

The similarity parameter of Sakurai[9] is expressed by

$$c_0 t / R_0 = f(R/R_0) \tag{18}$$

where c_0 denoted the undisturbed speed of sound, R the shock radius, and R_0 the characteristic length. A quasi-similarity rule was proposed by Oshima[24].

b. Solution of Bach and Lee (1970)

Bach and Lee[17] reported an approximate solution similar to that of Sakurai[26] for the entire range of the blast evolution (from strong shock to weak acoustic wave). The main assumption is that the density behind the shock wave in the blast obeys a power law, with the exponent being a function of time. A quasi-similarity exists for the decay coefficient θ for moderate blast strengths as (Higashino et al.[30])

$$\theta = \theta(\eta) \tag{19}$$

where

$$\theta \equiv R\ddot{R}/\dot{R}^2 \equiv \frac{R}{M_s}\left(\frac{dM_s}{dR}\right), \qquad \eta = 1/M_s^2 \tag{20}$$

As shown in **Fig.** 6a, the results for a spherical wave with $\gamma = 1.4$ for the shock decay confident θ (defined by eq. 20) agree closely with the numerical solution of Goldstine and Von Neumann[16]. The condition $\theta = -1$ corresponds to the strong shock limit, and $\theta = 0$ to the acoustic (weak shock) limit. Also shown in this plot are Sakurai's perturbation solution (Sakurai[14,15], and the approximate linear velocity profile solution of Sakurai[7].

The predicted pressure and particle velocity profiles are presented in **Figs.** 6b and 6c respectively for various values of the shock strength. The velocity profiles suggest that the particle velocities can be negative in regions behind the blast wave in the moderate and weak shock regions (i.e., particles are directed towards the center of symmetry). These results are consistent with the exact numerical solutions of Sedov[8].

3. ***The Shock Wave at Large Distance***

The similarity solutions were related to the description of strong shocks in the early stage of development (Sachdev). In the other extreme- the nearly linear regime, when the shock has become rather weak, Whitham[28] proposed a general theory to cover such flows. It describes attenuation of spherical shocks at large distances from the origin. The only assumption is that since the entropy changes are of third order in strength, the flow with weak shocks may be considered *isentropic*. Thus $R = R(c_0, t)$ at large distances form the origin. A fraction of explosion energy which is degraded as heat is thus not available for doing work as the shock propagates.

C. High Pressure Gas Explosions (Bursting Sphere)

A more realistic problem than that of point explosion is the case of a unit sphere of high pressure gas at time $t = 0$ suddenly expanding into a homogeneous atmosphere (air) at rest. This problem was treated numerically by Brode[18,19] and analytically (approximately) by Friedman[31]. At sufficiently high pressure, an important phenomenon arises here due to the occurrence of a secondary shock that does not appear in the one-dimensional shock tube problem (Sachdev[27]).

When a highly pressurized sphere is suddenly released, an *inward rarefaction wave* in the high-pressure region and *contact discontinuity* appears between the rarefaction wave and the shock wave (**Fig.** 7). At the contact discontinuity, the pressures and velocities on the two sides are the same, but the density and temperatures on the two sides are different. The contact discontinuity initially moves out behind the main shock front but with a decreasing velocity. A second shock wave can arise between the contact discontinuity and the rarefaction wave (Liu et al.[32]). In the 1-D shock tube problem, the main shock and the expansion wave come into instantaneous equilibrium being separated by a region of uniform pressure and velocity (Friedman[31]). Physically, the reason for the formation of the second shock is that the high pressure gas must expand to lower pressures than those reached through an equivalent one-dimensional expansion, due to the expansion of volume. On account of this overexpansion, the pressures at the tail of the rarefaction wave are lower than those transmitted back by the main shock, and a compression, or a second shock, must be inserted to connect the two phases. Because the second shock wave occurs in the expansion region, it is expected to be rather weak initially and propagate outwards with the expanding gas. However, its strength increases with time and reaches a fairly high intensity in a short time. Soon, the second shock wave stops propagating outwards and *comes to a halt* before reverting to implode on the origin.

A typical blast wave pressure profile is shown here (**Fig** 8). The major difference between a planar shock wave and a planar blast wave is that the flow properties behind the shock wave front are constant. A distinct characteristic of a spherical blast wave is a moving shock wave (jump in pressure) immediately accompanied by expansion waves behind the blast wave front, there is a blast wave profile region in which the flow properties are rapidly decreased due to expansion waves (Chen & Liang[25]). Due to its 3-D expansion, the intensity of the blast wave always decreases with time and distance during its propagation. The overpressure phase is due to the shock front and the under-pressure phase is due to the expanding waves following the shock front. Both phases result in two visible shock peaks on the pressure-time plot. By contrast in shock tube experiments, the pressure downstream of a shock wave is often constant between itself and the following contact surface.

1. ***Brode's Numerical Solutions***

Brode[18] simulated spherical blast waves, and considered two cases of practical importance: 1. strong shock, point-source explosions, 2. the sudden release of high pressure isothermal (both cold and hot) gas from spherical

enclosures. For the point explosion problem, he considered the exact solution of von Neumann[12] as an initial condition. Ideal gas equation of state is considered. Artificial viscosity, introduced by von Neumann and Richtmyer[33] is considered.

Brode[19], in a subsequent study, considered a blast wave from a spherical charge of TNT, with an equation of state for trichlorotoluene (TNT). In his numerical studies of detonation with a spherical charge of TNT, the existence of a second shock in the focal region was demonstrated. By considering real gas at high temperature, Brode[19] has shown that the blast over pressure at any radius is lower than that given by the ideal gas solution, since a part of the available energy is absorbed by the processes of ionization and dissociation.

Goldstine and von Neumann[16] and Brode[18] show that the variation of shock overpressure varies with the shock radius R follows a power law of the form

$$p - 1 = AR^n \tag{21}$$

where n is a slowly varying function of R, and A a constant (Sachdev[27], p. 242).

a. Brode's Solution for Blast Overpressure

Brode[19] has shown theoretically that the peak overpressure p_{s0} from a free spherical air blast can be expressed in dimensionless form (Wyle Labs[34])

$$\frac{p_{so}}{p_0} = f\left[\frac{d}{(E/p_0)^{1/3}}\right] = f(\lambda) \tag{22}$$

where p_{so} is the peak overpressure due to TNT explosion, p_0 the atmospheric pressure, λ the reduced distance, d the actual distance (ft), and E the energy of the blast (lbf.ft).

For standard atmospheric conditions,

$$\frac{E}{p_0} = \frac{W_T \text{x} 1.55\text{x}10^6}{2116} = 733 W_T \tag{23}$$

where W_T is the TNT equivalent weight (lb). Thus

$$p_{so} = f_2(Z) \tag{24a}$$

where

$$Z = d / W_T^{1/3} = 9.02\lambda \tag{24b}$$

For surface explosions, the blast parameters are equivalent to a free air blast with twice the energy of free air blast. Thus

$$Z = 2^{1/3} 9.02\lambda = 11.37\lambda$$

Fig. 9 represents a curve fit to Brode's numerical solution for the blast overpressure from TNT explosions as a function of Z. A power-law fit appears to be satisfactory. The numerical solution agrees with the test data on TNT and propellant explosions.

Fig. 10a shows the variation of shock Mach number and shock speed as a function of overpressure, as given by eq. (8a). The shock speed increases with increasing overpressure. For example, at an overpressure of 400 psia, the shock Mach number is about 5, with the shock speed being 5500 ft/s, which is comparatively high relative to the ambient sound speed (1100 ft/s). The dependence of particle velocity on overpressure is provided in **Fig.** 10b, as obtained form eq. (8b).

D. Spectral Characteristics and Detection of Blast Waves

Blast waves could be detected by a wideband microphone (Diaci[4]), who investigated the weak shock region. By analyzing blast wave signals in the *time and frequency domain*, the characteristic features of their nonlinear waveform evolution can be investigated. Many blast wave studies were concerned with the kinematic analysis of shock wave propagation, including shock position vs. time or shock velocity vs. time. The decay of blast wave amplitude (pressure, density or any other physical quantity) has been studied less often. Typical detected signals and their amplitude spectra are shown in **Fig.** 11. The basic signal waveform shows an initial positive part that corresponds to compression followed by a negative part attributed to rarefaction. The spectra exhibit typical bandpass characteristics with one central peak and approximately constant percentage bandwidth. The higher the amplitude, the larger the signal duration t_w. The higher the spectral amplitude peak, the lower the peak frequency.

The strong dependence of the waveform duration on the blast energy E_h is also reflected in the frequency domain. The spectral peak f_m increases as E_h decreases. The nonlinear broadening of the waveform due to shock wave propagation is observed. As the spherical blast wave propagates, the tail of the rarefaction gradually steepens and eventually a shock builds up there also. Asymptotically, the waveform evolves into the well-known symmetrical N-waveform with shock discontinuities in the front and the back. As a result of this distortion, ripples are introduced into the high frequency part of the spectrum.

The following section outlines general (nonformatting) guidelines to follow, drawn from the original AIAA Manuscript Preparation Kit. These guidelines are applicable to all authors (except as noted), and include information on the policies and practices relevant to the publication of your manuscript.

III. Interaction of Spherical Blast Waves (Blast Wave Coalescence)

Reported studies on interacting spherical blast waves are relatively few, although The interaction of a pair of (weak) cylindrical blast waves of either equal or unequal strength were studied experimentally and computationally by Higashinoet al.[30]. In sequential detonation and spatially distributed blast sources, it is known that shock waves coalesce and focusing can lead to significant amplification of peak overpressure. At sufficiently large distances from the charges, coalescence will occur. An overtaking wave may first encounter the negative overpressure phase of the wave being overtaken, causing it to decelerate. The overtaking wave must be somewhat stronger than the wave being overtaken or it will not be able to penetrate the negative overpressure phase and coalescence cannot occur. Once this phase has been penetrated and the overtaking wave has penetrated the positive phase of the wave being overtaken, coalescence takes place but occurs only after some additional propagation.

Several approximate methods of combining peak overpressure from N coalesced waves are described in Starkenberg and Benjamin[1] as follows:

A. Simple superposition

$$\Delta p = \sum_{i=1}^{N} \Delta p_i \tag{22}$$

where Δp represents the combined overpressure, and Δp_i the overpressure of blast wave i.

B. Full LAMB Model

Hikida and Needham[35] utilized the following scheme for blast coalescence.

$$\rho = \rho_0 + \sum_{i=1}^{N} \Delta\rho_i$$

$$U = \frac{\sum_{i=1}^{N} \rho_i U_i}{\rho} \tag{23}$$

$$\Delta p = \sum_{i=1}^{N} \Delta p_i + \frac{\gamma+1}{2}\left(\frac{1}{2}\sum_{i=1}^{N} \rho_i U_i^2 - \frac{1}{2}\rho U^2\right)$$

where ρ refers to density, and V the velocity of blast propagation.

C. Single Effective Charge

The method of single effective charge considers the use of pressure produced by the total explosive weight of all stacks with the coalesced waves combined at their centers of charge. That is, the peak overpressures associated with coalesced waves are essentially the same as those produced by single charges of the same total explosive weight. Zaker[36] experimentally showed that with three equal charges, the third pulse tends to overtake the second before the second overtakes the first.

Charges of equal/unequal mass (charges) and delay time, and separation distances need to be considered in the development of pressure combination algorithms and coalescence maps (patterns).

IV. Test Data on Overpressure

Blast overpressure data were obtained using scale model and full scale solid rocket propellant motors (upper stage) at NASA White Sands Test facility[37]. The solid propellant is struck by shaped charges of 500 gm and 20 gm. **Both** symmetrical (equal strength) and unsymmetrical (unequal strength) wave interactions were studied.

A. Scale Model Tests

1. ***Test Configuration and Instrumentation***

In the scale-model test, considered here, the propellant weight was 474 lb. For comparison, the full scale propellant in the full scale motor is about 4,431 lb. The configuration (**Fig.** 12a) includes a Ti-cylinder around the propellant stack to simulate the effects of the casing around the actual motor. The solid propellant was impacted with one 500-gm conical-shaped charge of C4 and 17 gm of Comp A-4 booster pellet. The burning of notable unburned propellant fragments that were collected is videotaped and timed. The data is recorded up to 45 sec. from the fire command (t = 0 sec).

The blast overpressure is measured by piezoelectric transducer pressure gauges (PCB) mounted on three adjustable elevated gauges lines (EGL), namely F, G and H, separated 120 deg. apart. EGL F and H are fitted with a flat plate at one end, with the PCB mounted in the plate center (thus measuring the stagnation overpressure, which includes both the static and dynamic components of overpressure (**Fig.** 12b). Five pairs of PCB's are flush mounted equal distances apart on each side of the pipe, in designated positions A and B. The PCB's are located 180 deg from each other, parallel to the ground. The EGL's are constructed from 4 in. diameter steel pipe, 30 ft. long, and are held 72 in. above the ground (parallel to). The PCB's have a 500 kHz resonant frequency, and a 1-μs rise time. Only the near-field blast pressure is measured.

2. ***Test Data for Overpressure***

Fig.13a shows the overpressure history for the stagnation overpressure from the closest gauge on EGL-F (channel-67), which is 4.92 ft from ground zero. This typical blast waveform is characterized by a peak overpressure (30 psia) at 16.2 ms, and positive pressure duration (about 1 ms). The stagnation overpressure includes a dynamic component due to the particle motion. We also notice a distinct wave due to propellant explosions, with a peak

overpressure of 16.4 psi at 19.2 ms. Only one major peak overpressure due to the propellant burn is observed here. The peak overpressure due to the charge is higher than that due to that of propellant. Both the blast overpressure and **the positive pressure duration** are consistent with the blast scaling due to Brode (1950). It is remarkable that the propellant pulse is wider than the pulse resulting from the 500-gm CSC. The relatively longer decay of the overpressure from the propellant blast is attributable to the long duration over which the energy is added to the flowfield. The overpressure phase is associated with the shock front location, and the under-pressure phase is linked to the expansion waves following the front.

The overpressure history for a number of locations along the EGL: F-A is demonstrated in **Fig.** 13b. This illustrates the propagation and attenuation of the blast wave. For example, considering the first two PCB's (separated by about 2 ft), the 500-gm peak is displaced by about 1 ms. This result is consistent with the shock speed of about 1500 ft/s (**Fig.**10a). The peak Δp diminishes from 30 psi at 4.9 ft to 2.5 psi at 23 ft.

Fig. 13c presents an extrapolation of the near-field Δp data from the near-field to the far-field covering distances (altitudes) from 25,000 ft. The Δp decay seems to be somewhat consistent with that indicated by the scaling laws.

B. Full Scale Propellant Test

1. ***Test Configuration and Instrumentation***

The full scale tests are described in WSTF Special Test Report[37]. **Fig.** 14a shows a photographic view of the actual motor. The overall dimensions of the test article were 5 ft wide x 7.5 ft tall with 4431 lb of propellant. The propellant composition is: 71 % ammonium perchlorate, 18 % aluminum powder, 11 % hydroxyl-termicrated polybutadiene binder (HTPB). The motor casing is fabricated from titanium alloy TI -6A1-4V. A total of four shaped charges (CSC) were used. An aft enclosure was used to simulate the nozzle. Two 500-gm shaped charges were used for the breakup system, mounted in the PAF oriented 180° from each other. Two 20-gm shaped charges were located in the spin table assembly, near the top of the nozzle skirt. The two 20-gm shaped charges were oriented 180° from each other in the same vertical plane as the 500-gm charges. For the PNH BUS, the 20-gm charges were located at azimuths of 191.3° and 338°, while the 500-gm charges were at 90° and 270°. All shaped charges were initiated in the timing sequence designed for the MER destruct system. In the MER BUS design, the 500-gm CSCs are initiated 0.87 ms after the 20-gm shaped charges are actuated. The PNH BUS timing sequence is similar.

The test set up and instrumentation is essentially similar to those described for the scaled propellant tests (**Fig.** 14b). The instrumentation for the full scale testing is similar to that in the scaled tests, except the charges are not symmetric for EGL-F and EGL-G.

2. ***Test Data for Overpressure***

Fig. 15a illustrates the history from the stagnation transducer on EGL-F (channel-67). It indicates a series of blast waves. Two 20-gm charges are followed by two 500-gm charges in succession. The peak Δp due to 500-gm is considerably higher than that due to 20-gm peaks, since the energies are different, as indicated by the scaling law (Appendix-A.1). For the EGL-F the two 500-gm are separated by about 4 ft., and travel at about 2300 ft/s, so that $\Delta t \approx 1.7$ ms (the measured Δt is about 1.7 ms). The peak Δp related to propellant explosion are superposed on to the 500-gm charge waveforms, and the peak magnitude (about 20 psi) are consistent with those for the scaled model test. Also secondary shock waves are noted. The 20-gm charges do not seem to have initiated any significant propellant burn (or breakup), with more localized rather than large-scale action.

The peak Δp history for various locations along the EGL-F (**Fig.** 15b) suggests that the 500-gm charges ultimately coalesce at about 20 sec. This merging of shocks is a consequence of the fact that the trailing shock travels relative to the particle motion occasioned in the wake of the leading shock; thus it moves at a higher speed for the same strength. The Δp decreases from 65 psi to 7.5 psi as the distance increases (due to spherical spreading). The strength of the merged shock is due to the two charges. There seems to be a problem (data drop out) with channel 37 after about 12 sec.

The characteristics of the blast propagation for EGL: F-B (B-side transducer) is seen to be similar to that of EGL: F-A in all respects (**Fig.** 15c). This is to be expected, as the transducers are similarly situated. This demonstrates the consistency of measurements. Likewise, in the case of EGL-G (**Fig.** 15d), the behavior is similar to that of EGL-F, since the charges are similarly situated. In the case of EGL-H (**Fig.** 15e), the two 500-gm charges are located equidistantly relative to the gauges, so that the two peaks are very close.

The spectral distribution of energy for the pressure signal from channel 67 (F-A) for individual explosions of short duration for the various explosions (20 gm charge, 500 gm charge, and propellant explosion) are depicted in **Fig.** 16. It is seen that the energy is distributed over a broad range of frequencies, as is to be expected for impulse type functions typical of the blast wave. There is some spectral similarity for the various explosions, with the spectra displaying a distinct peak. The spectra are similar to those presented for blast waveforms (Diaci and Mozina 1992).

Fig. 17 presented the extrapolation of peak pressures to the far-field. The extrapolation suggests that the peak pressures at about 25,000 ft are discernible, thus pointing to the feasibility of the ground microphone system for on-board explosion detection. However, the occurrence of multiple explosions, blast wave coalescence, and absorption of sound at high frequency and over long distances should be taken into account.

V. Conclusions

Both the scaled test data and full scale propellant blast test data have been helpful in our understanding of the blast propagation from single and multiple charges. The data illustrate the effects of blast coalescence and propagation of blast waves of different strength. An examination of the test data suggests that the test data for blast overpressure are generally consistent with the available blast scaling laws. Further work is in progress with regard to the interaction effects of blast waves.

Acknowledgments

Geoffrey Rowe (ASRC) assisted with the LabView software in the spectral representation of some of the WSTF test data.

References

[1]Starkenberg, J.K.., and Benjamin, K.J., "Predicting coalescence of blast waves from sequentially exploding ammunition stacks," Army Research Lab Report ARL-TR-645, December 1994.

[2]Taylor, G.I., "The air wave surrounding an expanding sphere," *Proceedings of the Royal Society* A, Vol. 186, 1946, p. 273.

[3]**Diaci**, J., and Mozina, J., In *Physical Acoustics: Fundamentals and Applications*, ed. O. Leroy, and M.A.. Breazeale, Plenum, NewYork, 1991, p. 291.

[4]Diaci, J., and Mozina, J., "A study of blast wave forms detected simultaneously by a microphone and a laser probe during laser ablation,"*Applied Physics*, Vol. A55, 1992, pp. 352-358.

[5]Taylor, G.I., "The formation of a blast wave by a very intense explosion, I," *Proceedings of the Royal Society, Ser.* A, Vol. 201, 1950, pp. 159-174.

[6]Taylor, G.I., "The formation of a blast wave by a very intense explosion, II. The atomic explosion of 1945," *Proceedings of the Royal Society, Ser.* A, Vol. 201, 1950, p. 175.

[7]Sakurai, A., Blast Wave Theory, in *Basic Developments in Fluid Dynamics* (ed. M. Holt), Academic Press, New York, 1965, pp. 309-375.

[8]Sedov, L.I., *Similarity and Dimensional Methods in Mechanics*, Academic Press, New York, Chap. 4, 1959 (10th ed., CRC Press, London, 1993).

[9]Oppenheim, A.K., Kuhl, A.L., and Lundstrom, E.A., "A parametric study of self-similar blast waves," *Journal of Fluid Mechanics*, Vol. 52, Pt. 4, 1972, pp. 657-682.

[10]Kinney, G.F., *Explosive Shocks in Air*, Springer-Verlag, 1962 (also see Kinney, G.F. and Graham, K.J., 2nd ed., 1985).

[11]Sedov, L.I., "Propagation of intense (strong) blast waves," *Prikl. Mat. Mek. (PMM)*, Vol.10, 1946, p.241 (in Russian).

[12]Von Neumann, J., "The point source solution," National Defense Research Committee, Div. B Report AM-9 (see Collected Works of J. von Neumann, Vol. VI, Pergamon Press, Oxford, 1947, p. 219).

[13]Director, M.N., and Dabora, E.K., "Predictions of variable-energy blast waves," *AIAA Journal*, Vol. 15, No. 9, 1977, pp. 1315-1321.

[14]Sakurai, A., "On the propagation and the structure of the blast wave I," *Journal of the Physical Society of Japan*, Vol. 8., 1953, p. 662.

[15]Sakurai, A., "On the propagation and the structure of the blast wave II," *Journal of the Physical Society of Japan*, Vol. 9, 1954, p. 256.

[16]Goldstine, H.H., and von Neumann, J., "Blast wave calculation," *Communications in Pure and Applied Mathematics*, Vol. 8, 1955, pp. 327-354.

[17]**Bach, G.G.**, and Lee, J.H.S., "An analytical solution of blast waves," *AIAA Journal*, Vol. 8, 1970, p. 271.

[18]Brode, H.L., "Numerical solutions for spherical blast waves," *Journal of Applied Physics*, Vol. 26, 1955, pp. 766-775.

[19]Brode, H.L., "Blast wave from a spherical charge," *Physics of Fluids*, Vol. 2, No. 2, 1959, pp. 217-229.

[20]Shapiro, A., *The Dynamics and Thermodynamics of Compressible Fluid Flow*, John Wiley, New York, 1953.

[21]Liepmann, H.W., and Roshko, A., *Elements of Gas Dynamics*, John Wiley & Sons Inc, 1957, p. 63.

[22]Taylor, J.L., "An exact solution of the spherical blast wave problem," *Philosophical Magazine*, Vol. 46, 1955, p. 317.

[23]Landau, L.D., and Lifshitz, E.M., *Fluid Mechanics*, 2nd ed., Pergamon Books Ltd., London, 1987.

[24]Oshima, K., "Blast waves produced by exploding wire,"Aero. Res. Inst., University of Tokyo, Rept. 358-26-9, 1960.

[25]Chen, H., and Liang, S.M., "Planar blast/vortex interaction and sound generation," *AIAA Journal*, Vol. 40, No. 11, 2002, pp. 2298-2304.

[26]**Sakurai**, A., "Exploding wires based on a conf. Exploding wire phenomena," **in** (W.G. Chace and H.K. Moore, eds.), I, Plenum Press, New York, 1959.

[27]Sachdev, P.L., *Shock Waves and Explosions*, Chapman & Hall/CRC, New York, 2000.

[28]Whitham, G.B., "The propagation of spherical blast," Rept. 358, Aeronautical Research Institute, Univ. of Tokyo, Japan, July 1960.

[29]Landau, L.D., "On shock waves at a large distance from the place of their origin," *Soviet Journal of Physics*, Vol. 9, 1945, p. 496.

[30]Higashino, F., Henderson, L.F., and Shimizu, F., "Experiments on the interaction of a pair of cylindrical weak blast waves in air, " *Shock Waves*, Vol. 1, 1991, pp. 275-284.

[31]Friedman, M.P., "A simplified analysis of spherical and cylindrical blast waves," *Journal of Fluid Mechanics*, Vol. 11, 1961, pp.1-15.

[32]Liu, T.J., Khoo, B.C., and Yeo, K.S., "The numerical simulations of explosion and implosion in air: Use of a modified Harten's TVD scheme,"*International Journal for Numerical Methods in Fluids*, Vol. 31, 1999, pp. 661-680.

[33]Von Neumann, J., and Richtmeyer, R.D., "A method for the numerical calculation of hydrodynamic shocks," *Journal of Applied Physics*, Vol. 21, 1950, pp. 232-237.

[34]Wyle Laboratories, Sonic and vibration environments for ground facilities – A design manual, Report No. WR 68-2, March 1968.

[35]Hikida, S., and Needham. L.E., "Low Altitude Multiple Burst (LAMB) Model," S-cubed Final Report, S-CUBED-R-81-5067, 30 June 1981.

[36]Zaker, T.A., "Farfield overpressure from closely spaced sequential detonations," 11th Explosive Safety, 9-10 September 1969

[37]NASA White Sands Test Facility, "STAR 48B Full Scale Demonstration Test'" Special Test Report WSTF # 02-36952, October 29, 2002.

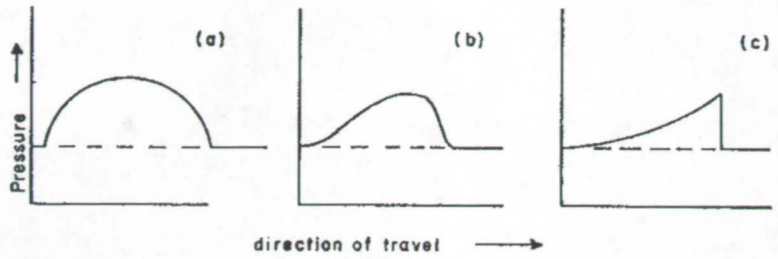

Fig. 1 Temporal evolution of a blast wave

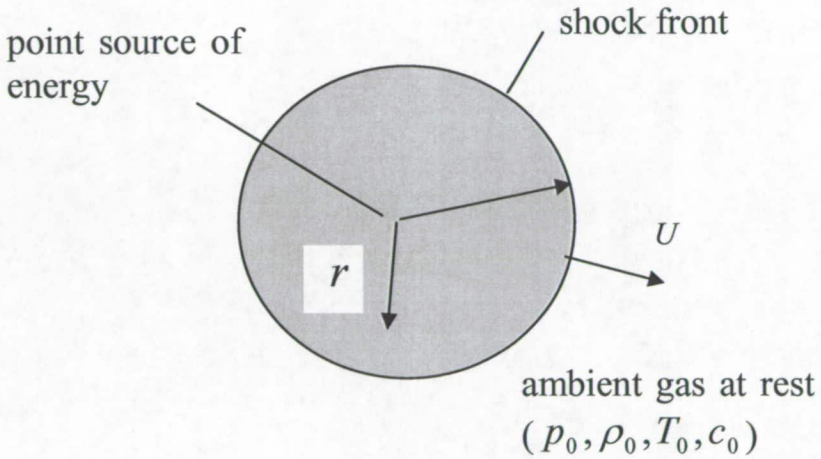

Fig. 2a Schematic of a point source explosion

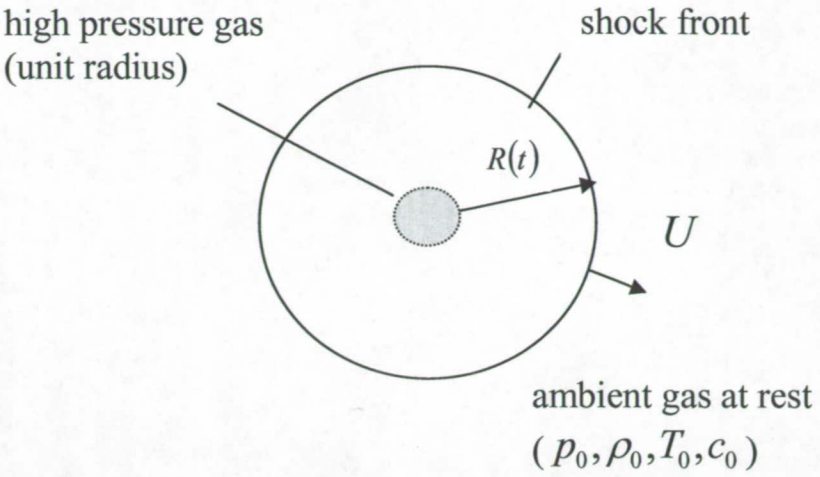

Fig. 2b Schematic of an explosion of an initially spherical charge.

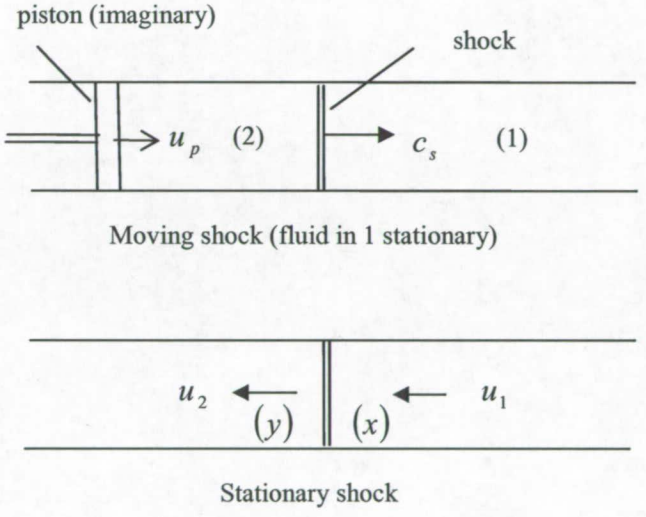

$$c_s = u_1$$

$$u_p = u_1 - u_2$$

Fig. 3 Propagating and stationary shocks (adapted from Liepmann & Roshko, 1957).

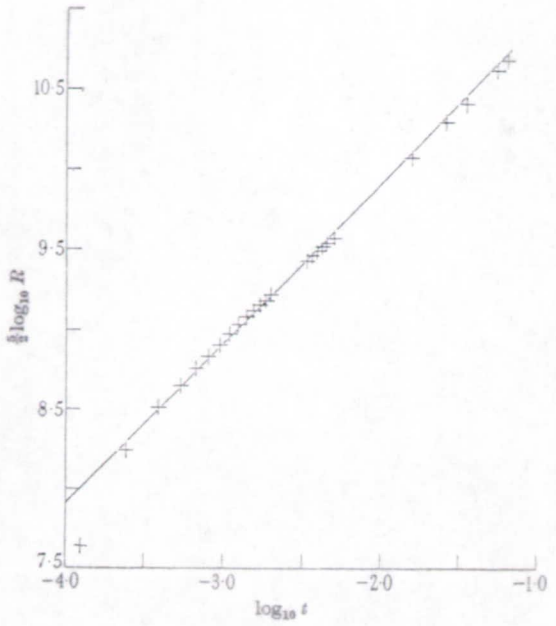

Fig. 4a Variation of shock radius with time for the strong shock solution of Taylor (1946).

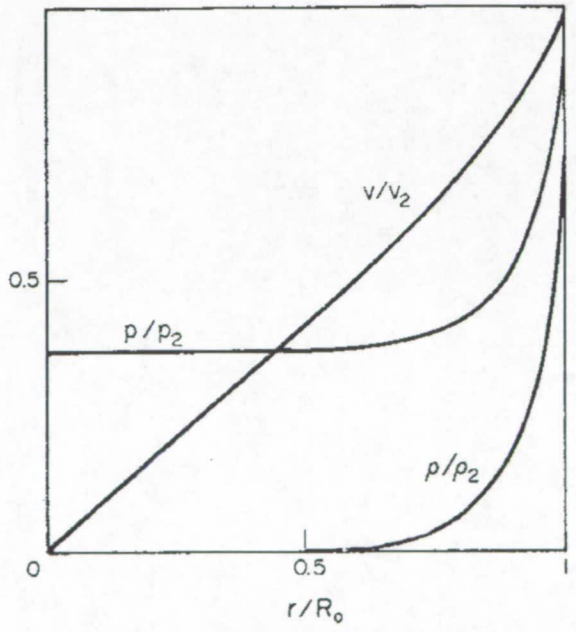

Fig. 4b The strong shock solution of Sedov (1946).

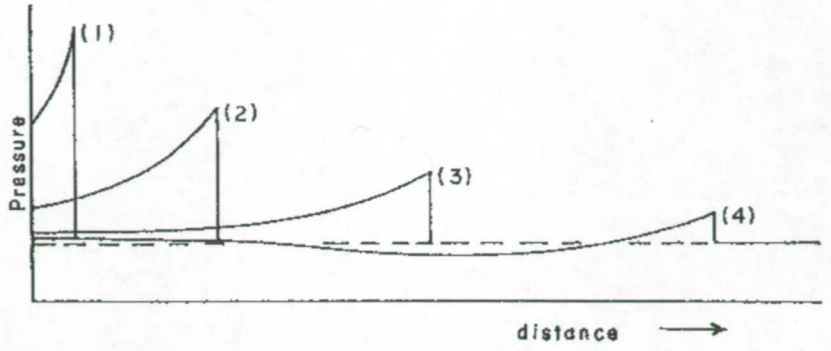

Fig. 5a Spatial distribution of pressure at various times for intermediate shock strength (adpated from Kinney 1962).

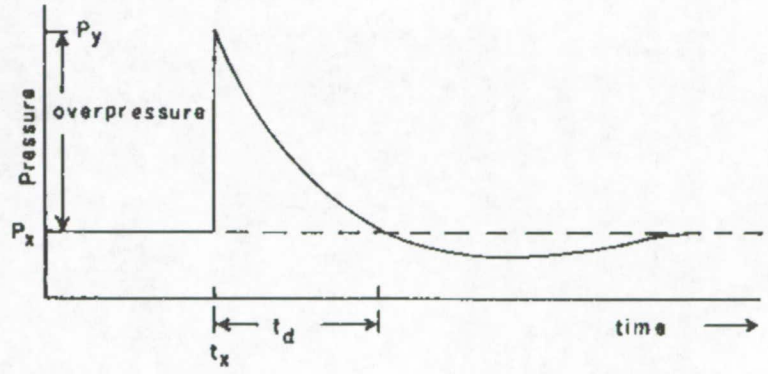

Fig. 5b Pressure-time varaition of a blast wave of moderate shock strength (adapted from Kinney 1962).

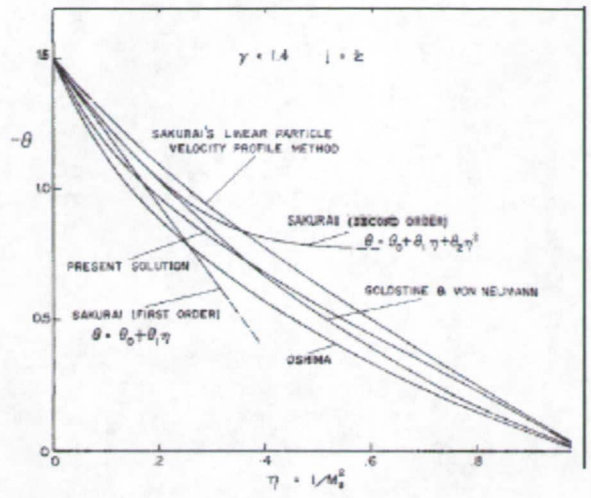

Fig. 6a Comparison of shock decay coefficient for shocks of moderate strength (Bach & Lee 1970).

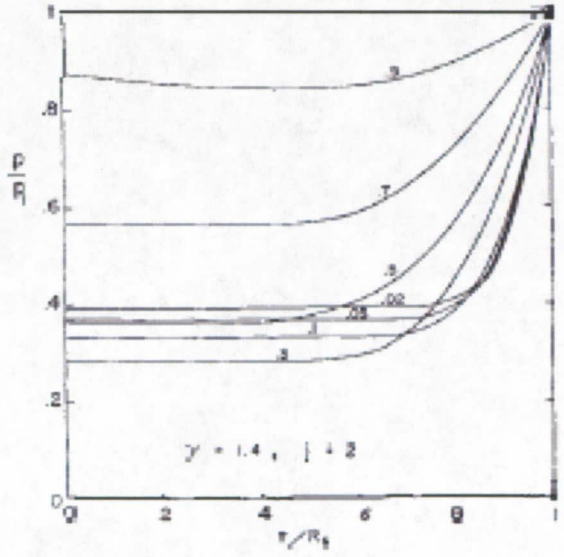

Fig. 6b Pressure distribution behind the shock for various times (Bach & Lee 1970).

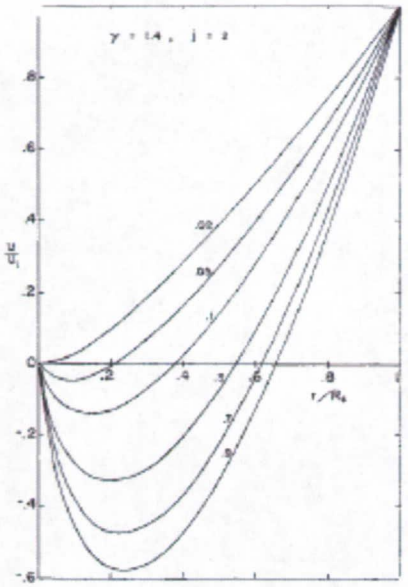

Fig. 6c Particle velocity distribution at various time (Bach & Lee 1970).

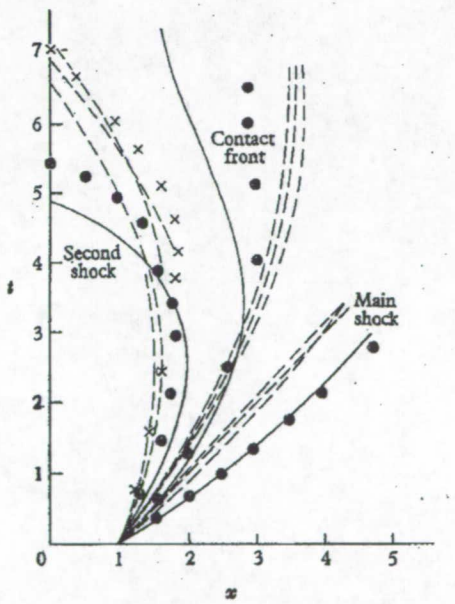

Fig. 7 Comparison of shock positions for the explosion of a spherical charge (Friedman 1971).

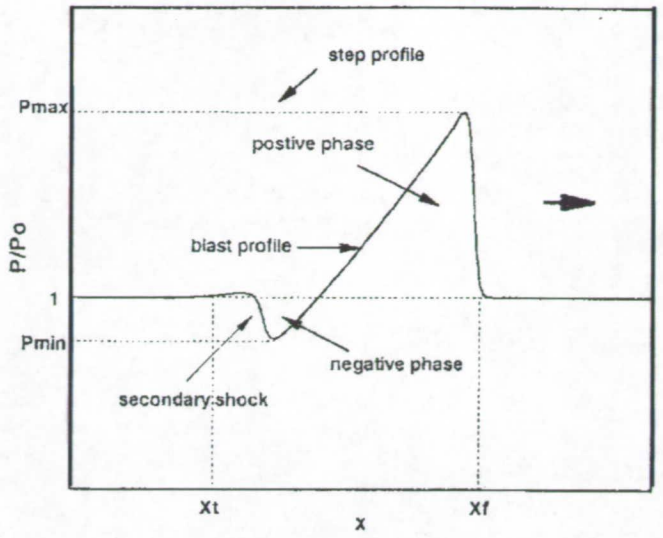

Fig. 8 A typical blast wave from a spherical charge, showing secondary shock.

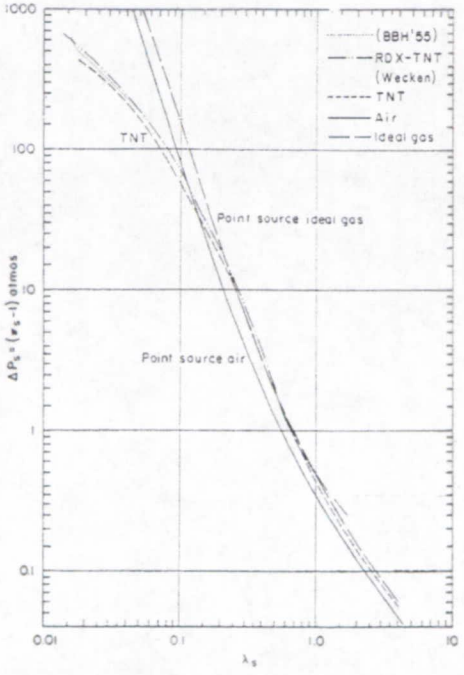

Fig. 9 Brode's numerical solution for shock overpressure (Brode 1959).

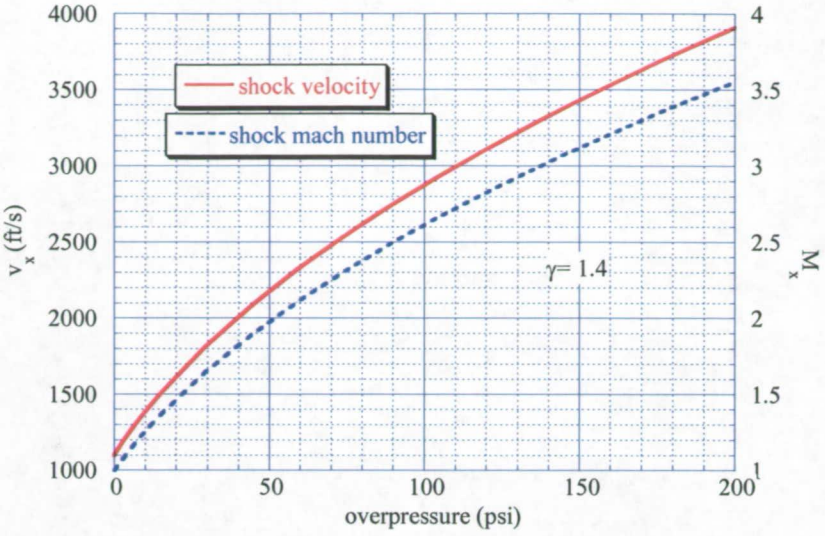

Fig. 10a Shock velocity and shock Mach number from Rankin-Hugonoit reations.

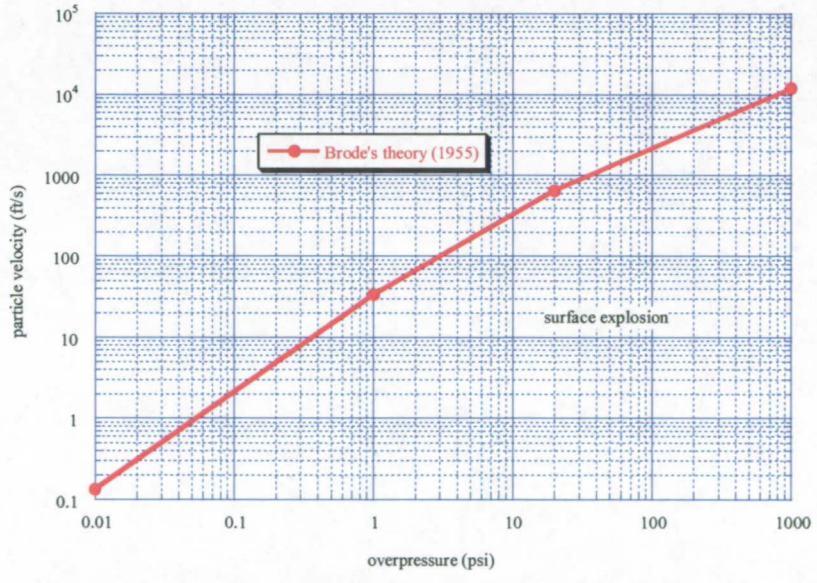

Fig. 10b Particle velocity for blast wave propagation.

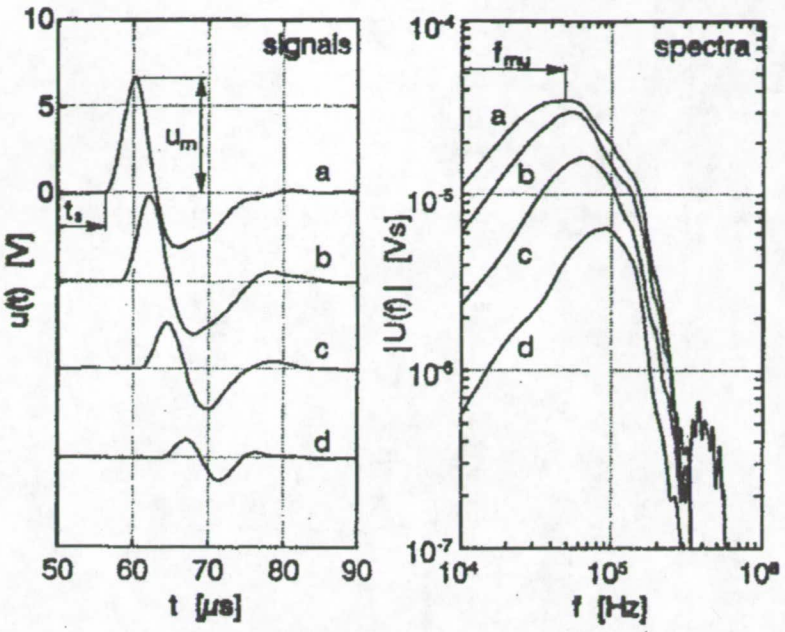

Fig. 11 Spectral characteristics of blast waves (Diaci 1992).

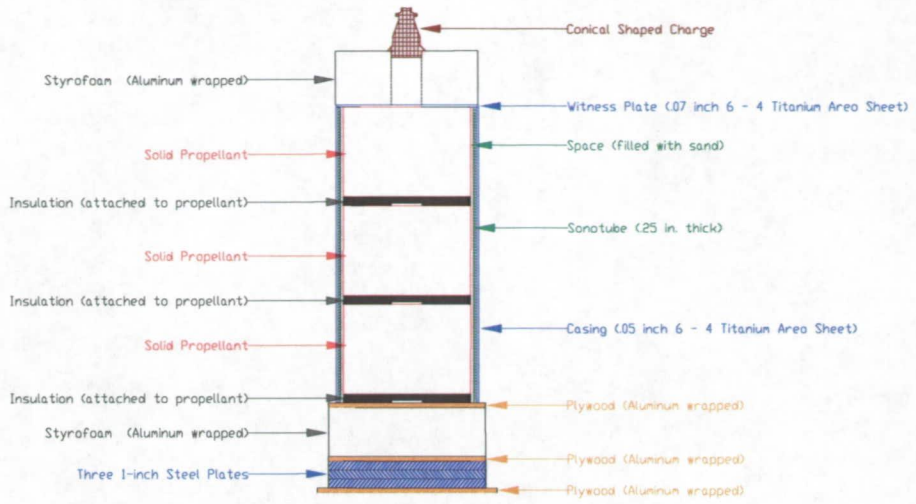

Fig. 12a Test set up for scaled testing.

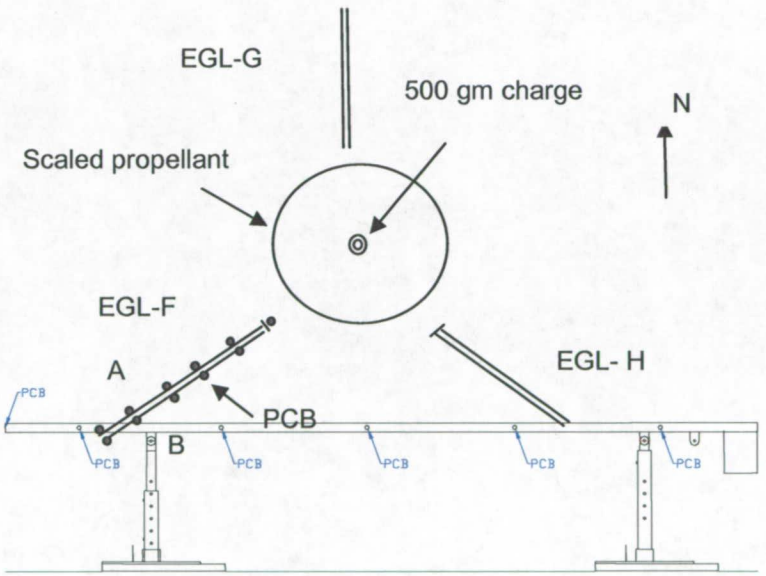

Fig. 12b EGL and PCB locations for scaled test.

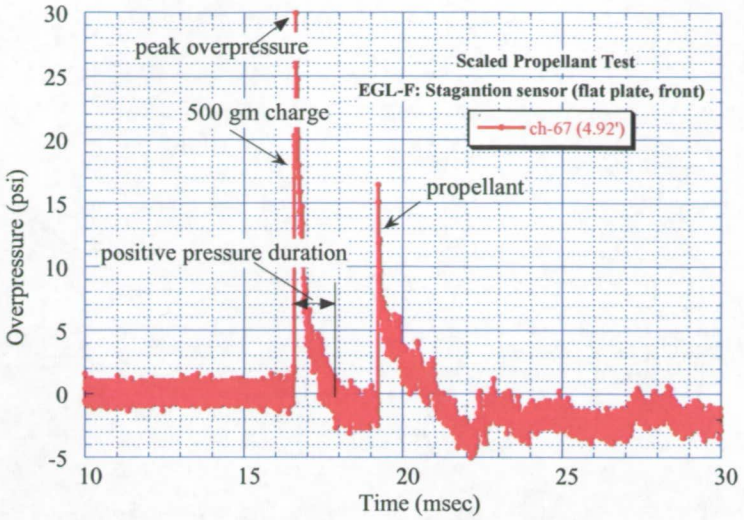

Fig. 13a Overpressure history at the stagnation location for the scaled test.

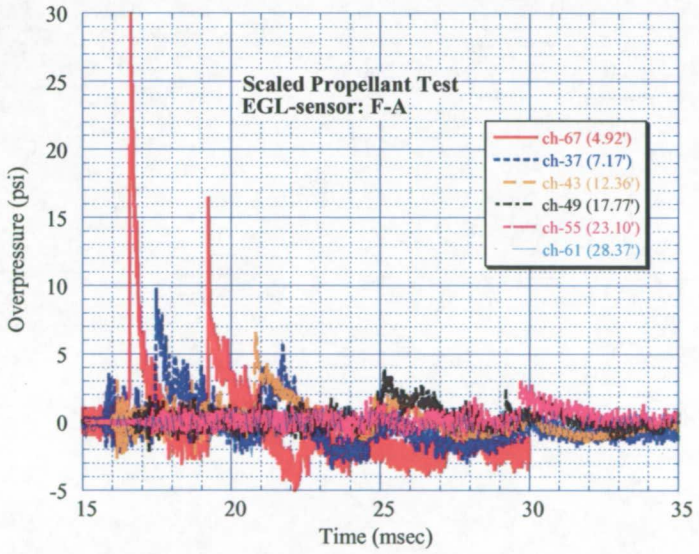

Fig. 13b Overpressure history for the scaled test (contd.).

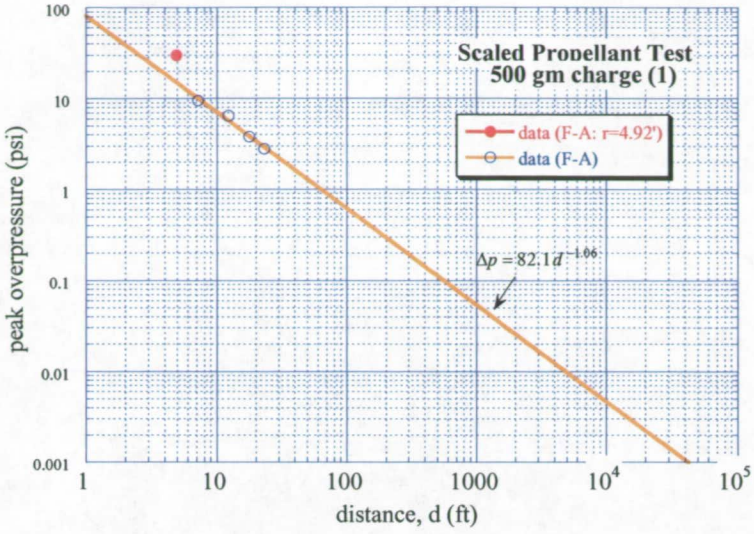

Fig. 13c Peak overpressure scaling for the scaled test data.

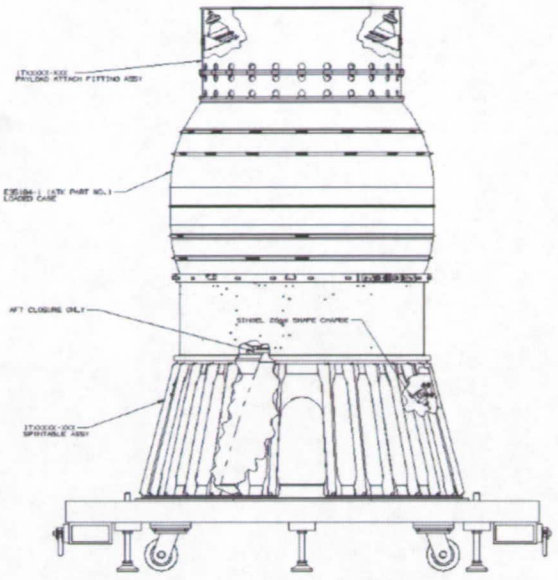

Fig. 14a Full scale test setup.

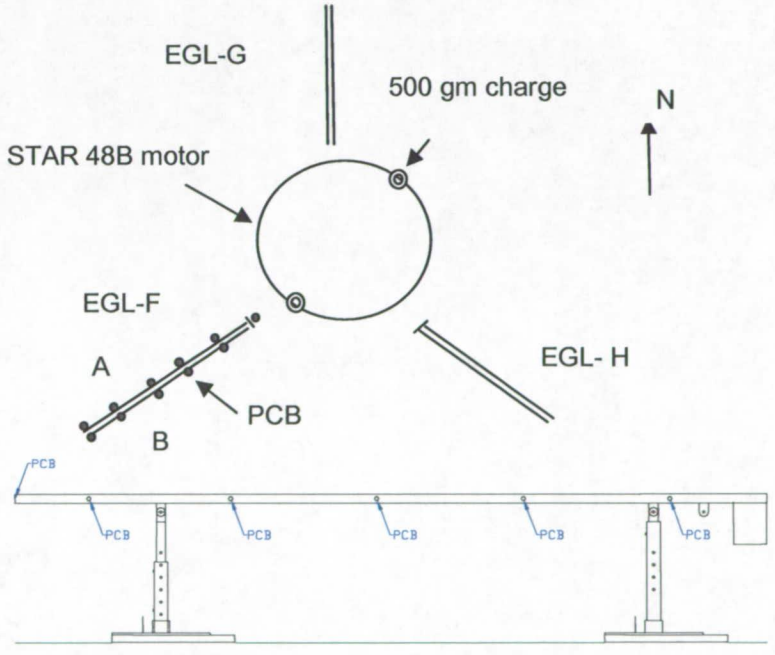

Fig. 14b EGL and PCB locations for full scale testing.

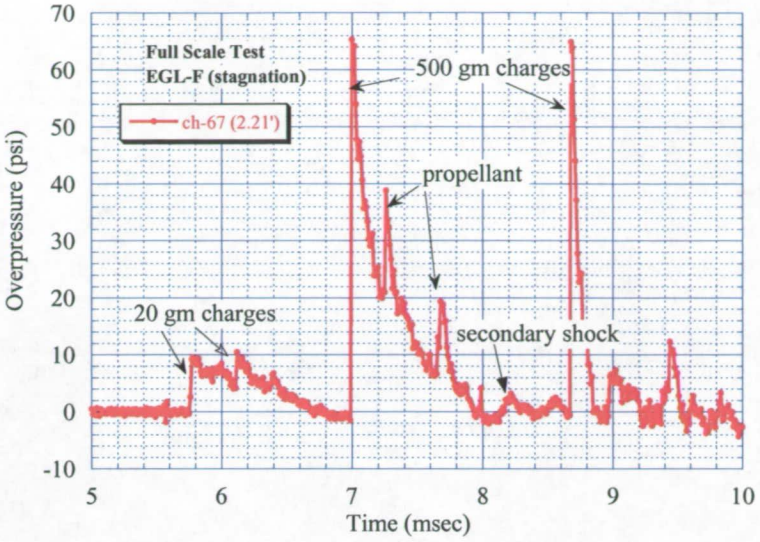

Fig. 15a Overpressure history at the stagnation point for full scale testing.

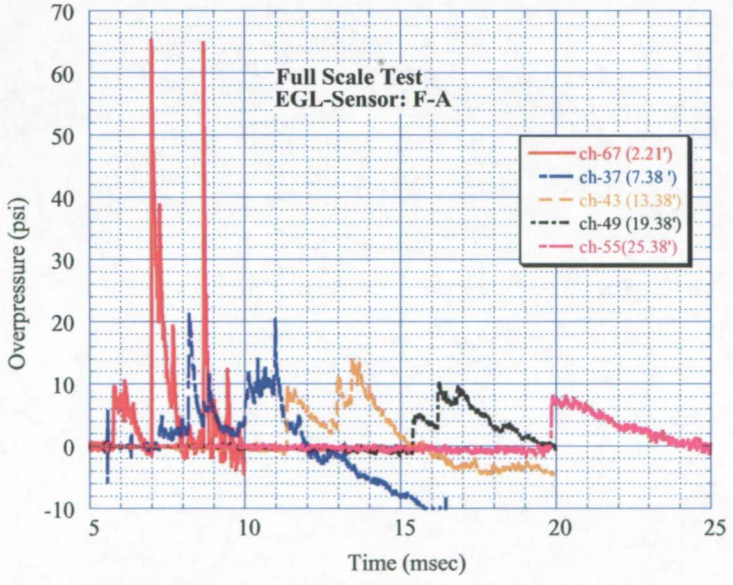

Fig. 15b Overpressure history of sensors along F-A for full scale testing.

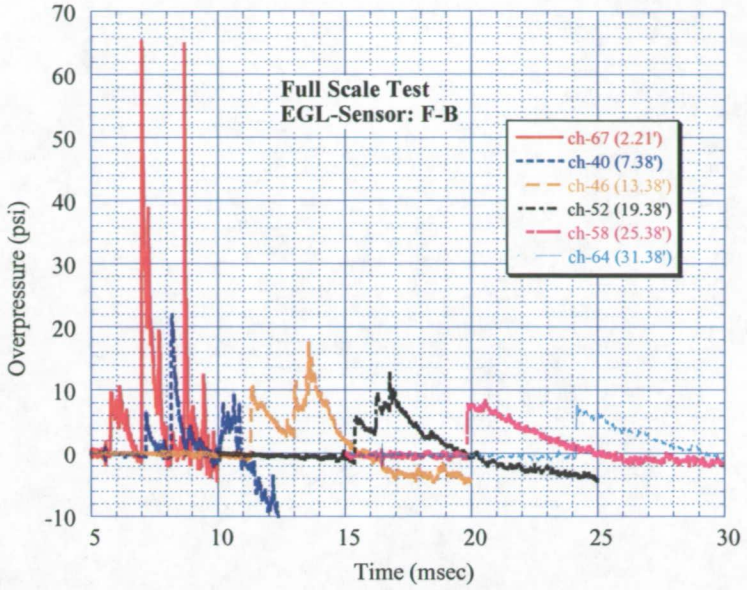

Fig. 15c Overpressure history of sensors along F-Bfor full scale testing.

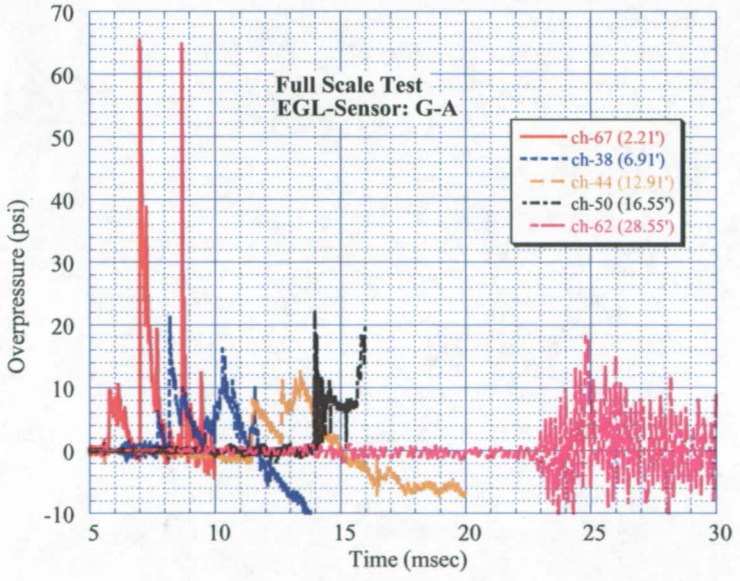

Fig. 15d Overpressure history of sensors along G-A for full scale testing.

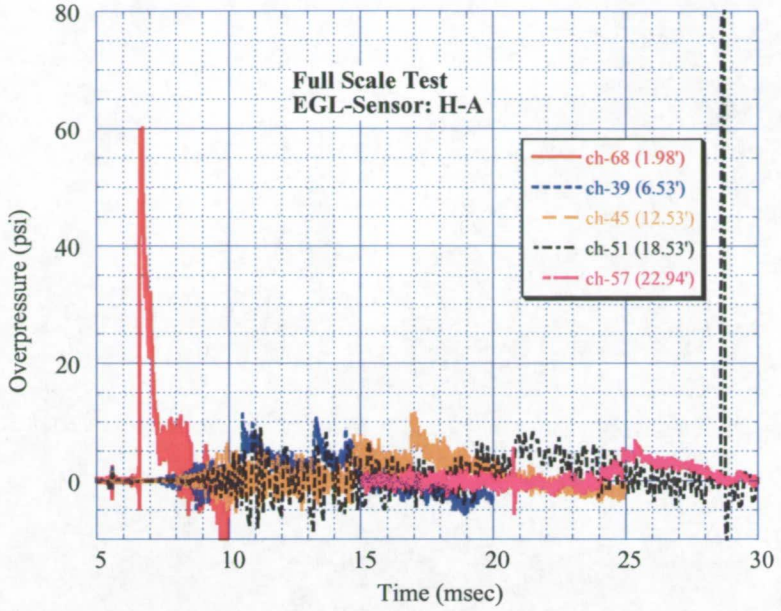

Fig. 15e Overpressure history of sensors along H-A for full scale testing.

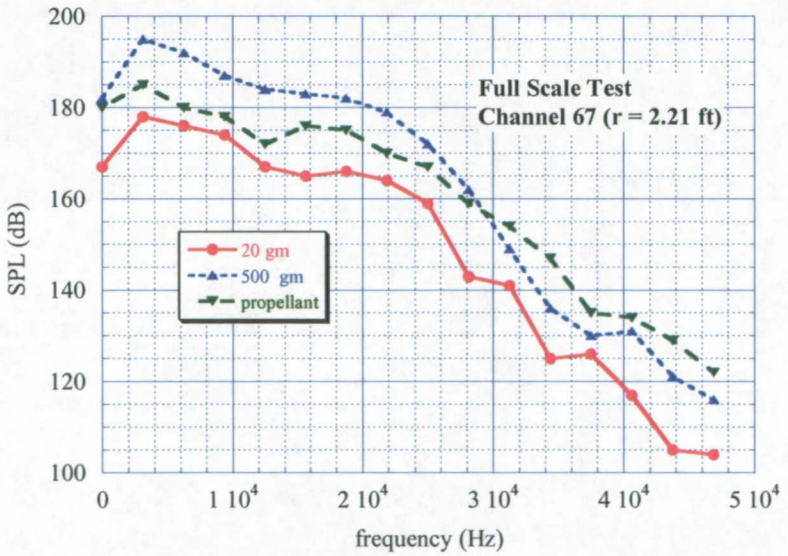

Fig. 16 Spectral distribution for full scale testing.

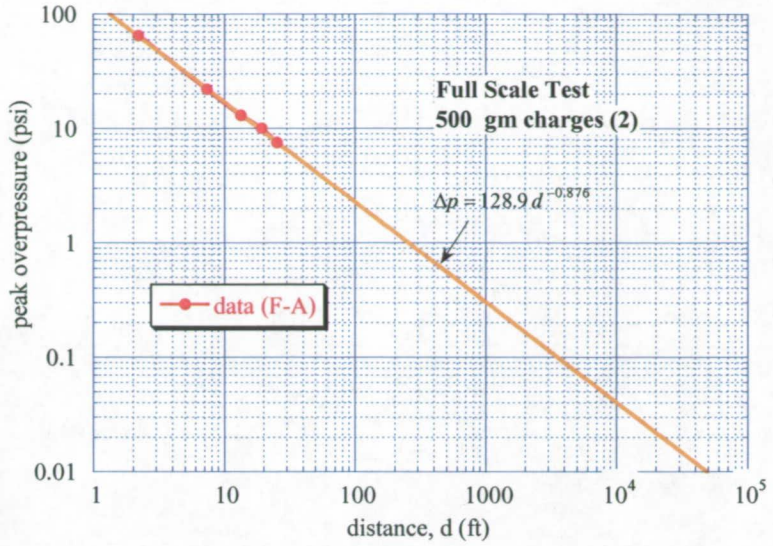

Fig. 17 Peak overpressure scaling for full scale testing.

REPORT DOCUMENTATION PAGE

Form Approved
OMB No. 0704-0188

PLEASE DO NOT RETURN YOUR FORM TO THE ABOVE ADDRESS. RETURN COMPLETED FORM TO

1. REPORT DATE *(DD-MM-YYYY)*	2. REPORT TYPE	3. DATES COVERED *(From - To)*
	Conference/Journal Article	25/28-06-2007

4. TITLE AND SUBTITLE	5a. CONTRACT NUMBER
On the Propagation and Interaction of Spherical Blast Waves	NAS10-03006
	5b. GRANT NUMBER
	5c. PROGRAM ELEMENT NUMBER

6. AUTHOR(S)	5d. PROJECT NUMBER
Max Kandula and Robert Freeman	5e. TASK NUMBER
	5f. WORK UNIT NUMBER

7. PERFORMING ORGANIZATION NAME AND ADDRESS	8. PERFORMING ORGANIZATION REPORT NUMBER
USTDC, Sierra Lobo, Inc. Fluid System Design, ASRC-5211 Kennedy Space Center, FL 3289	

9. SPONSORING/MONITORING AGENCY NAME(S) AND ADDRESS(S)	10. SPONSOR/MONITOR'S ACRONYM(S)
National Aeronautics and Space Administration Launch Services Program (VA) Kennedy Space Center, FL 32899	NASA/KSC
	11. SPONSOR/MONITOR'S REPORT NUMBERS(S)

12. DISTRIBUTION AVAILABILITY STATEMENT

13. SUPPLEMENTARY NOTES

14. ABSTRACT

The characteristics and the scaling laws of isolated spherical blast waves are briefly reviewed. Both self-similar solutions and numerical solutions of isolated blast waves are discussed. Blast profiles in the near-field (strong shock region) and the far-field (weak shock region) are examined. Particular attention is directed at the blast overpressure and shock propagating speed. Consideration is also given to the interaction of spherical blast waves. Test data for the propagation and interaction of spherical blast waves emanating from explosives placed in the vicinity of a solid propellant stack are presented. These data are discussed with regard to the scaling laws concerning the decay of blast overpressure.

15. SUBJECT TERMS

blast waves, propagation of blast waves, spherical blast waves, solid propellant stack, coalescence of blast waves, blast wave scaling laws

16. SECURITY CLASSIFICATION OF:			17. LIMITATION OF ABSTRACT	18. NUMBER OF PAGES	19a. NAME OF RESPONSIBLE PERSON
a. REPORT	b. ABSTRACT	c. THIS PAGE			Max Kandula
				32	19b. TELEPHONE NUMBER *(include area code)* (321) 383-9996